CHAPTER ONE

INTRODUCTION

A solar domestic hot water (SDHW) system consists of solar collectors, heat exchangers, storage tanks, auxiliary heaters, pipes, pumps, valves, and controllers. It absorbs solar radiation in collectors, delivers the collected energy to the thermal storage tank with or without heat exchangers, and then provides hot water for domestic usage. Excess thermal energy is stored in one or two thermal storage tanks. When the solar energy is insufficient to meet the heating load, an auxiliary heater will provide the thermal energy. Figure 1.1 shows a schematic diagram of a typical one-tank forced-circulation SDHW system.

To evaluate the performance of solar heating systems, experimental or numerical testing methods can be used. While experiments yield valuable information, numerical modeling allows differentiating between designs at reasonable costs. A simulation program like TRNSYS [7] needs performance equations or data for each component to perform system simulation. The main objective of this study is to develop a design

program that can reproduce the performance of the flat-plate solar collectors. At the development level the design program can replace physical experimental tests with numerical tests. In addition, it can be used as the design tool for a company specializing in SDHW systems. In this thesis a design program is developed so that very detailed

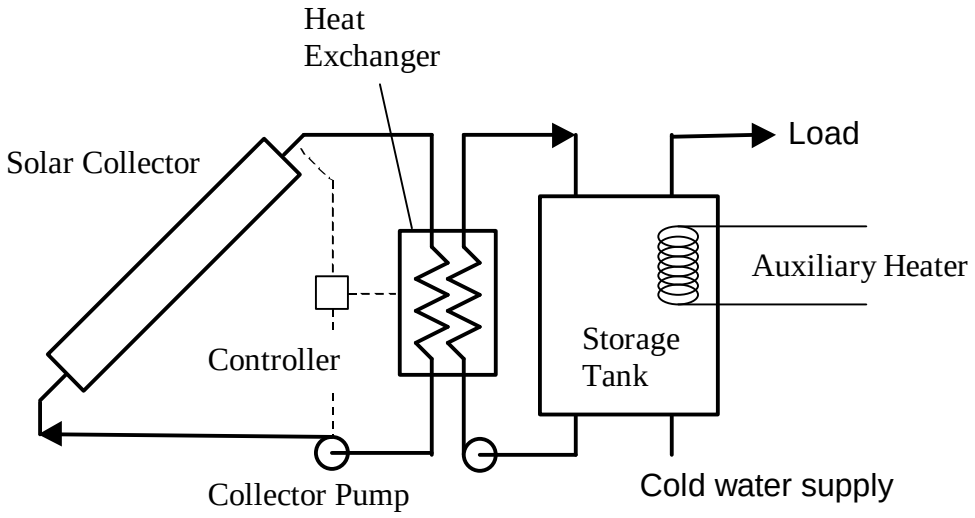

Figure 1.1 Schematic of a typical solar domestic hot water system

information can be specified to allow solar engineers to investigate the impact of design changes on the collector performance.

1.1 Flat-Plate Solar Collectors

Flat-plate solar collectors have potential applications in many space-heating situations, air conditioning, industrial process heat, and also for heating domestic water [3]. These collectors use both beam and diffuse radiation. A well-designed collector can produce hot water at temperature up to the boiling point of water [3]. They are usually fixed in position permanently, have fairly simple construction, and require little maintenance. To keep costs at a level low enough to make solar heating more attractive than other sources of heat, the materials, dimensions, and method of fabrication must be chosen with care.

A flat-plate solar collector consists of a radiation-absorbing flat plate beneath one or more transparent covers, tubes attached to the plate to transport the circulating fluid and back and edge insulation to reduce heat loss. Water or an anti-freeze fluid circulates through the collector by a pump or by natural convection to remove the absorbed heat.

Even though the theory of flat-plate solar collectors is well established, accurate design programs, which have an easy-to-use graphic interface and include all the design factors, are not available. In this thesis a detailed model is developed that includes all of the design features of the collector such as: plate material and thickness, tube diameters and spacing, number of covers and cover material, back and edge insulation dimensions, etc. The program is useful for collector design and for detailed understanding of how collectors function. For system simulation programs such as TRNSYS [7], simple models such as instantaneous efficiency and incident angle modifier are usually adequate. The detailed model developed in this study can provide these simple parameters.

1.2 Engineering Equation Solver

Engineering Equation Solver (EES) is a program developed by Professor Sanford A. Klein of the Solar Energy Laboratory, University of Wisconsin – Madison

[6]. It can solve a system of algebraic, differential, and complex equations. It can also perform optimization, provide linear and nonlinear regression, and generate publication-quality plots. Since it automatically identifies and groups equations to be solved simultaneously, the solver always operates at optimum efficiency. Many mathematical functions, thermophysical properties, and transport properties are also provided by built-in functions that are helpful in solving engineering problems in thermodynamics, fluid mechanics, and heat transfer. With these features, the user is able to concentrate more on his/her own problem. EES is particularly useful for design problems in which the impacts of one or more parameters need to be investigated.

The professional version of EES provides multiple diagram windows and additional features by which a programmer can develop graphic user interface. One valuable feature of the professional version is "make distributable." Once a program is developed, a compiled version can be created. This compiled version can be freely distributed among students and the solar engineers. The design programs of this study will be developed with EES.

1.3 Objectives

The objective of this thesis is to develop a new analytical and modeling tool to evaluate the performance of components in order to reduce the cost of solar domestic hot water (SDHW) systems. The new design tool will allow engineers to make design changes and determine their effects on the thermal performance at a reasonable cost. The program will be arranged so that very detailed information can be specified. It will allow a company specializing in SDHW systems to investigate the impact of design changes in their equipment on the thermal performance. For the task to be useful to the SDHW industry, the design program will have to provide performance equations and data that can be used a system simulation program like TRNSYS [7]. The program should also provide comparisons of the analytical results from EES with experiments following SRCC [17] practice that are normally performed on solar collector. Throughout the project, it is necessary to ensure that EES is capable of modeling and analyzing innovative designs.

CHAPTER TWO

FLAT-PLATE SOLAR COLLECTORS

A solar collector is a very special kind of heat exchanger that uses solar radiation to heat the working fluid. While conventional heat exchangers accomplish a fluid-to-fluid heat exchange with radiation as a negligible factor, the solar collector transfers the energy from an incoming solar radiation to a fluid. The wavelength range of importance for flat-plate solar collectors is from the visible to the infrared [3]. The radiation heat transfer should be considered thoroughly in the calculation of absorbed solar radiation and heat loss. While the equations for collector performance are reduced to relatively simple forms in many practical cases of design calculations, they are developed in detail in this thesis to obtain a thorough understanding of the performance of flat-plate solar collectors.

2.1 Physical Model For Flat-Plate Solar Collectors

e MSC-

ıc. [13].

e solar

SC-32 Flat-plate solar collector. American Energy Technologies Inc.(from FRSC test report [13])

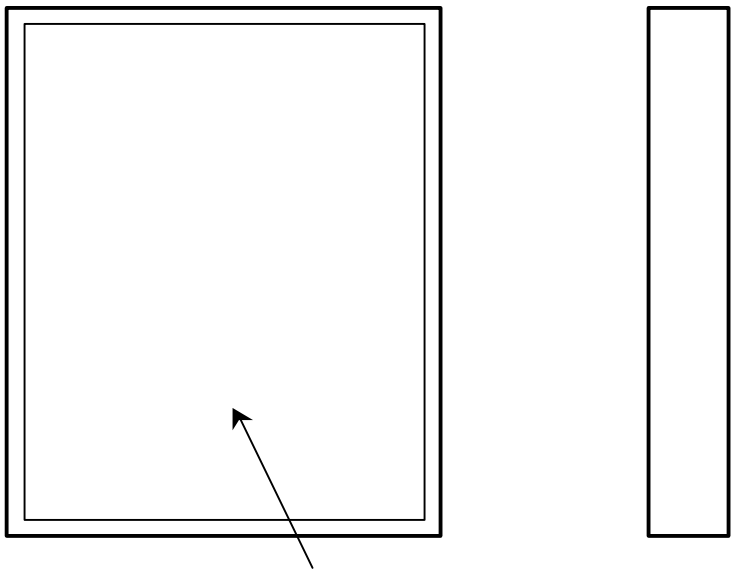

(a) Frontal view (b) Side view

Figure 2.1.2 Physical flat-plate collector model

collector. Important parts are the cover system with one or more glass or plastic covers, a plate for absorbing incident solar energy, parallel tubes attached to the plates, and

edge and back insulation. The detailed configuration may be different from one collector to the other. However, the basic geometry is similar for almost flat-plate solar collectors. The analysis of the flat-plate solar collector in this chapter is performed based on the configuration shown in Figure 2.1.2.

Some assumptions made to model the flat-plate solar collectors are as follows:

1. The collector operates in steady state.
2. Temperature gradient through the covers is negligible.
3. There is one-dimensional heat flow through the back and side insulation and through the cover system.
4. The temperature gradient around and through tubes is negligible.
5. The temperature gradient through the absorber plate is negligible.
6. The collector may have zero to two covers.
7. The semi-gray radiation model is employed to calculate radiation heat transfer in the solar and infrared spectrum.
8. In calculating instantaneous efficiency, the radiation is incident on the solar collector with fixed incident angle.

9. The collector is free-standing.

10. The area of absorber is assumed to be the same as the frontal transparent area.

2.2 Energy Balance Equation

In steady state, the performance of a flat-plate solar collector can be described by the useful gain from the collector, Q_u, which is defined as the difference between the absorbed solar radiation and the thermal loss or the useful energy output of a collector:

$$Q_u = \left[A_p S - A_c U_L \left(T_{pm} - T_a\right)\right]^+ \tag{2.2.1}$$

where A_c and A_p are the gross and aperture area of the collector, respectively. The first term is the absorbed solar energy and the second term represents the heat loss from the collector. The solar radiation absorbed by a collector per unit area of absorber S can be calculated using the optical properties of covers and a plate. The thermal energy loss from the collector to the surroundings can be represented as the product of a heat transfer coefficient U_L times the difference between the mean absorber plate temperature T_{pm} and the ambient temperature T_a. The + superscript indicates that only positive values of the terms in the square brackets are to be used. Thus, to produce useful gain greater than zero the absorbed radiation must be greater than the thermal

losses. Two collector areas appear in Equation 2.2.1; gross collector area A_c is defined as the total area occupied by a collector and the aperture collector area A_p is the transparent frontal area.

ASHRAE Standard [1] employs the gross area as a reference collector area in the definition of thermal efficiency of the collector. The useful gain from the collector based on the gross collector area becomes

$$Q_u = A_c\left[S_c - U_L\left(T_{pm} - T_a\right)\right]^+ \tag{2.2.2}$$

where S_c is the absorbed solar radiation per unit area based on the gross collector area, defined as

$$S_c = S\frac{A_p}{A_c}. \tag{2.2.3}$$

Since the radiation absorption and heat loss at the absorber plate is considered based on the aperture area in this study, it is convenient to make the aperture collector area the reference collector area of the useful gain. Then Equation 2.2.1 becomes

$$Q_u = A_p\left[S - U_L'\left(T_{pm} - T_a\right)\right]^+ \qquad (2.2.4)$$

where $U¢_L$ is the overall heat loss coefficient based on the aperture area given by

$$U_L' = U_L \frac{A_c}{A_p}. \qquad (2.2.5)$$

2.3 Solar Radiation Absorption

The prediction of collector performance requires knowledge of the absorbed solar energy by the collector absorber plate. The solar energy incident on a tilted collector consists of three different distributions: beam radiation, diffuse radiation, and ground-reflected radiation. The details of the calculation depend on which diffuse-sky model is used. In this study the absorbed radiation on the absorber plate is calculated by isotropic sky model [8]:

$$S = I_b R_b (ta)_b + I_d (ta)_d \left(\frac{1+\cos b}{2} \right) + (I_b + I_d)(ta)_g r_g \left(\frac{1+\cos b}{2} \right) \quad (2.3.1)$$

where the subscripts *b*, *d*, and *g* represent beam, diffuse, and ground-reflected radiation, respectively. I is intensity of radiation on a horizontal surface, (ta) the transmittance-absorptance product that represents the effective absorptance of the cover-plate system, and b the collector slope. r_g is the diffuse reflectance of ground and the geometric factor R_b is the ratio of beam radiation on the tilted surface to that on a horizontal surface. This section treats the way to calculate the transmittance-absorptance product of beam, diffuse, ground-reflected radiation for a given collector configuration and specified test conditions.

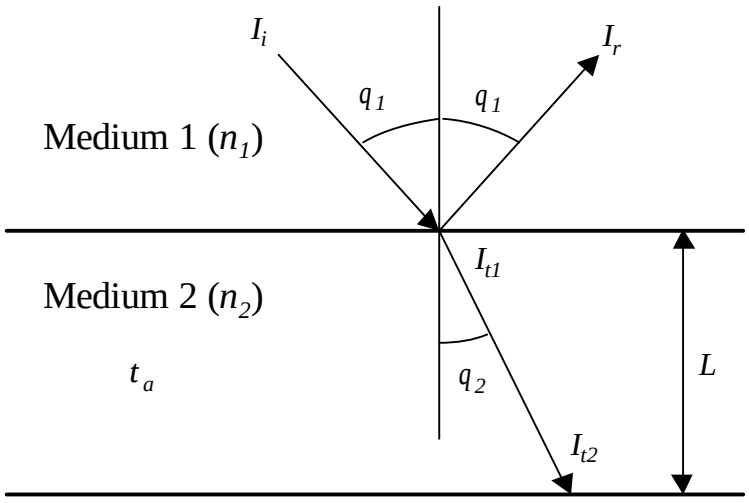

Figure 2.3.1 Incident and refraction angle and absorption in media

2.3.1 Reflection of Radiation

For a smooth interface the Fresnel equations evaluate the reflection of unpolarized radiation on passing from medium 1 with a refractive index n_1 to medium 2 with refractive index n_2 (Figure 2.3.1). The reflection of unpolarized radiation r is given by

$$r = \frac{I_r}{I_i} = \frac{1}{2}\left(r_{\perp} + r_{\parallel}\right) \tag{2.3.2}$$

where the perpendicular and parallel components are given by

$$r_{\perp} = \frac{\sin^2(q_2 - q_1)}{\sin^2(q_2 + q_1)} \tag{2.3.3}$$

$$r_{\parallel} = \frac{\tan^2(q_2 - q_1)}{\tan^2(q_2 + q_1)} \tag{2.3.4}$$

where q_1 and q_2 are the incident and refraction angles, respectively, that are related to the refraction indices by Snell's law:

$$\frac{n_1}{n_2} = \frac{\sin q_2}{\sin q_1}. \tag{2.3.5}$$

If the angle of incidence and refractive indices of media are known, the reflectance of a surface can be calculated by using Equations 2.3.2-2.3.5.

2.3.2 Absorption by Glazing

Bouguer's law [3] describes the absorption of radiation in a partially transparent medium. With the assumption that the absorbed radiation is proportional to the local intensity in the medium and the distance *x* the radiation has traveled in the medium, the

transmittance of the medium can be represented as (Figure 2.3.1)

$$t_a = \frac{I_{t2}}{I_{t1}} = \exp\left(-\frac{KL}{\cos q_2}\right) \tag{2.3.6}$$

where K is the extinction coefficient and L the thickness of the medium (Figure 2.3.1). The subscript a is a reminder that only absorption has been considered.

2.3.3 Optical Properties of Cover Systems

In the case of collector covers and windows, the solar radiation travels through a slab of materials. A cover or a window has two interfaces per cover causing reflection losses. At an off-normal incident angle, reflection is different for each component of polarization so that the transmitted and reflected radiation will be polarized. Ray tracing techniques [12] for each component of polarization yields the transmittance of initially unpolarized radiation.

The transmittance t, reflectance r, and the absorptance a of a single cover for incident unpolarized radiation can be found by the average of the perpendicular and parallel components of polarization:

$$t = \frac{1}{2}\left(t_{\perp} + t_{\parallel}\right), \quad r = \frac{1}{2}\left(r_{\perp} + r_{\parallel}\right), \quad a = \frac{1}{2}\left(a_{\perp} + a_{\parallel}\right) \tag{2.3.7}$$

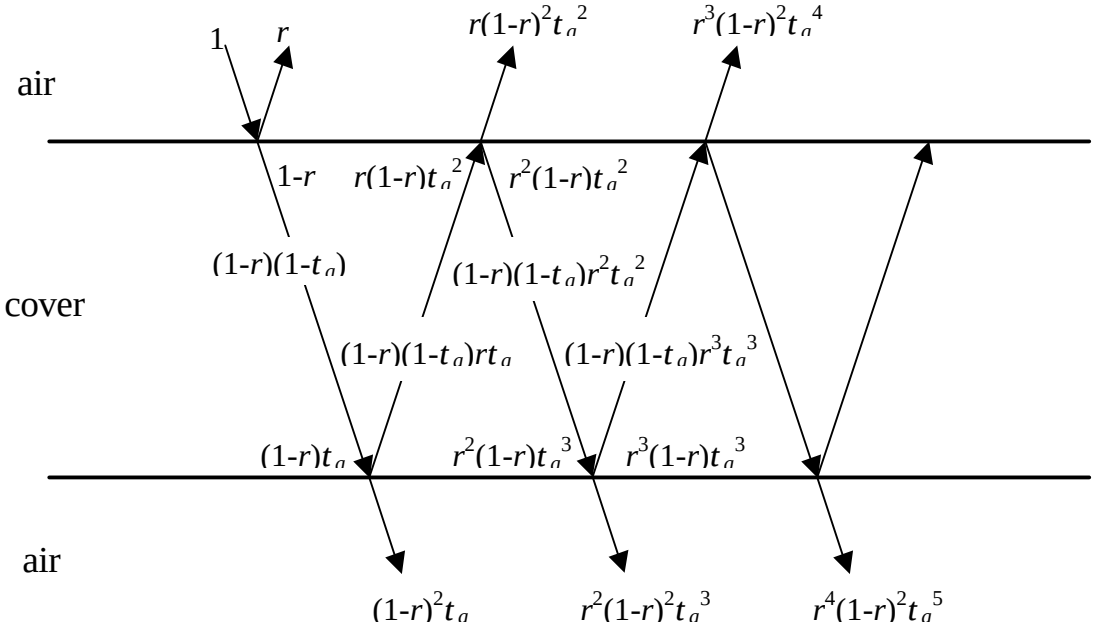

Figure 2.3.2 Ray-tracing techniques for transmittance and reflectance of a cover

where the perpendicular and parallel components of polarization can be determined by ray-tracing (Figure 2.3.2) as:

$$t_{\perp} = t_a (1-r)^2 \sum_{n=0}^{\infty} (r t_a)^{2n} = \frac{t_a (1-r_{\perp})^2}{1-(r_{\perp} t_a)^2} = t_a \frac{1-r_{\perp}}{1+r_{\perp}} \frac{\left(1-r_{\perp}^{\,2}\right)}{1-(r_{\perp} t_a)^2}$$

$$r_{\perp} = r_{\perp}\left[1+(1-r_{\perp})^2 t_a^{\,2} \sum_{n=0}^{\infty} (r_{\perp} t_a)^{2n}\right] = r_{\perp}\left[1+\frac{(1-r_{\perp})^2 t_a^{\,2}}{1-(r_{\perp} t_a)^2}\right] \qquad (2.3.8)$$

$$a_{\perp} = (1-t_a)(1-r_{\perp}) \sum_{n=0}^{\infty} (r_{\perp} t_a)^n = \frac{(1-t_a)(1-r_{\perp})}{1-r_{\perp} t_a}$$

$$t_{\parallel} = \frac{t_a (1-r_{\parallel})^2}{1-(r_{\parallel} t_a)^2} = t_{\parallel} \frac{1-r_{\parallel}}{1+r_{\parallel}} \frac{\left(1-r_{\parallel}^{\,2}\right)}{1-(r_{\parallel} t_a)^2}$$

$$r_{\parallel} = r_{\parallel}\left[1+(1-r_{\parallel})^2 t_a^{\,2} \sum_{n=0}^{\infty} (r_{\parallel} t_a)^{2n}\right] = r_{\parallel}\left[1+\frac{(1-r_{\parallel})^2 t_a^{\,2}}{1-(r_{\parallel} t_a)^2}\right] \qquad (2.3.9)$$

$$a_{\perp} = (1-t_a)(1-r_{\parallel}) \sum_{n=0}^{\infty} (r_{\parallel} t_a)^n = \frac{(1-t_a)(1-r_{\parallel})}{1-r_{\parallel} t_a}.$$

For a two-cover system ray-tracing yields the following equations for transmittance and reflectance [3]:

$$t = \frac{1}{2}\left(t_{\perp} + t_{\parallel}\right) = \frac{1}{2}\left[\left(\frac{t_2 t_1}{1 - r_2 r_1}\right)_{\perp} + \left(\frac{t_2 t_1}{1 - r_2 r_1}\right)_{\parallel}\right] \tag{2.3.10}$$

$$r = \frac{1}{2}\left[\left(r_2 + \frac{t r_1 t_2}{t_1}\right)_{\perp} + \left(r_2 + \frac{t r_1 t_2}{t_1}\right)_{\parallel}\right] \tag{2.3.11}$$

where subscript *1* and *2* refer to inner and outer cover, respectively. It should be noted that the reflectance of the cover system depends upon which cover first intercepts the solar radiation.

2.3.4 Equivalent Angles of Incidence for Diffuse Radiation

In the present sky radiation model, the radiation incident on a collector consists of beam radiation from the sun, diffuse solar radiation that is scattered from the sky, and ground-reflected radiation that is diffusely reflected from the ground. While the preceding analysis can be applied directly to beam contribution, the transmittance of

cover systems for diffuse and ground-reflected radiation must be calculated by integrating the transmittance over the appropriate incidence angles with an assumed sky model. The calculation can be simplified by defining equivalent angles that give the same transmittance as for diffuse and ground-reflected radiation [3].

Brandemuehl and Beckman [2] have performed the integration of the transmittance over the appropriate incident angle with an isotropic sky model and suggested the equivalent angle of incidence for diffuse radiation:

$$\theta_{d,e} = 59.7 - 0.1388\beta + 0.001497\beta^2 \qquad (2.3.12)$$

where β is the tilted angle of solar collector. For ground-reflected radiation, the equivalent angle of incidence is given by

$$\theta_{g,e} = 90 - 0.5788\beta + 0.002693\beta^2 . \qquad (2.3.13)$$

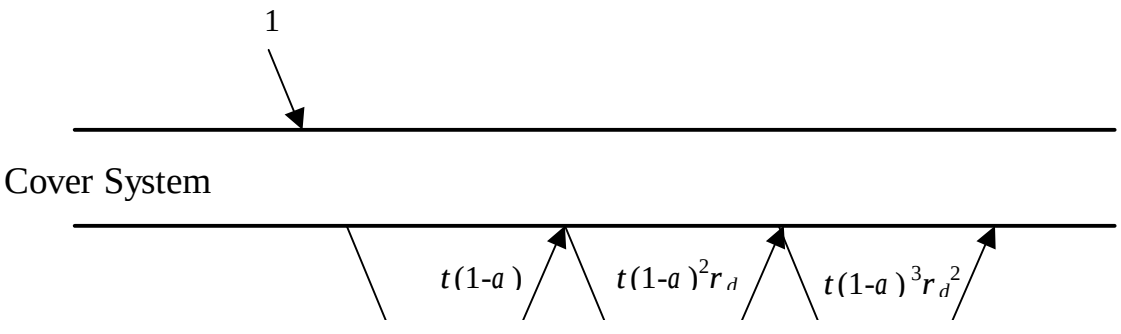

Figure 2.3.3 Absorbed solar radiation at the absorber plate

2.3.5 Transmittance-Absorptance Product ($\tau\alpha$)

Some of the radiation passing through the cover system is reflected back to the cover system while the remainder is absorbed at the plate. In turn, the reflected radiation from the plate will be partially reflected at the cover system and back to the plate as illustrated in Figure 2.3.3. In this figure, τ is the transmittance of the cover system at the desired angle, α is the angular absorptance of the absorber plate, and ρ_d refers to the

reflectance of the cover system for diffuse radiation incident from the bottom side. It is assumed that the reflection from the absorber plate is diffuse and unpolarized. The multiple reflection of diffuse radiation continues so that the fraction of the incident energy ultimately absorbed becomes

$$(\tau\alpha) = \tau\alpha \sum_{n=0}^{\infty} [(1-\alpha)\rho_d]^n = \frac{\tau\alpha}{1-(1-\alpha)\rho_d} \tag{2.3.14}$$

where ρ_d can be estimated from Equation 2.3.7 or Equation 2.3.11 at an angle of 60^o [3].

2.3.6 Angular Dependence of ($\tau\alpha$)

The angular dependence of transmittance-absorptance product can be found using Equation 2.3.1 - 2.3.11 for optical properties of covers and angular dependence relation for the absorptance of absorber plate. While the angular dependence of solar absorptance of most absorber surfaces is not available, Pettit and Sowell [11] have suggested that selective surfaces may exhibit similar behavior. In this study, a representative example of angular dependence relation from Duffie and Beckman [3] is

employed for angles of incidence between zero and 80^{o}:

$$\frac{a}{a_n} = 1 - 1.5879\times10^{-3}q + 2.7314\times10^{-4}q^2 - 2.3026\times10^{-5}q^3 + 9.0244\times10^{-7}q^4 - 1.8\times10^{-8}q^5 + 1.7734\times10^{-10}q^6 - 6.9937\times10^{-13}q^7 \quad (2.3.15)$$

where the subscript *n* refers to the normal incidence and q is in degrees.

2.4 Heat Loss From The Collector

In solar collectors, the solar energy absorbed by the absorber plate is distributed to useful gain and to thermal losses through the top, bottom, and edges [3]. In this section the equations for each loss coefficient are derived for a general configuration of the collector. The semi-gray model is employed for radiation heat transfer. All the optical properties in this section are for infrared radiation while Section 2.3 deals with the visible radiation.

2.4.1 Collector Overall Heat Loss

Heat loss from a solar collector consists of top heat loss through cover systems and back and edge heat loss through back and edge insulation of the collector. With the assumption that all the losses are based on a common mean plate temperature T_{pm}, the overall heat loss from the collector can be represented as

$$Q_{loss} = U_L A_c \left(T_{pm} - T_a \right) \tag{2.4.1}$$

where U_L is the collector overall loss coefficient. The overall heat loss is the sum of the top, back, and edge losses:

$$Q_{loss} = Q_t + Q_b + Q_e . \tag{2.4.2}$$

where the subscripts *t*, *b*, and *e* represent for the top, back, and edge contribution, respectively.

2.4.2 Top Heat Loss through the Cover System

To evaluate the heat loss through the cover systems, all of the convection and radiation heat transfer mechanisms between parallel plates and between the plate and the sky must be considered as shown in Figure 2.4.1. The collector model may have up to two covers and the cover system have 9 different combinations of covers: no covers,

one plastic cover, one glass cover, one glass (inner) and one plastic (outer) cover, one plastic (inner) and one glass (outer) cover, two glass cover, and two plastic cover. In case of plastic covers that are partially transparent to infrared radiation the direct radiation exchange between the plate and sky through the cover system must be considered while it is neglected for the glass covers since glass is opaque to infrared radiation. Whillier [19] has developed equations for top loss coefficients for the collector cover system using radiation heat transfer coefficients. In this study the net radiation method [12] is applied to obtain the expression for the heat loss for the general cover system of flat-plate solar collectors.

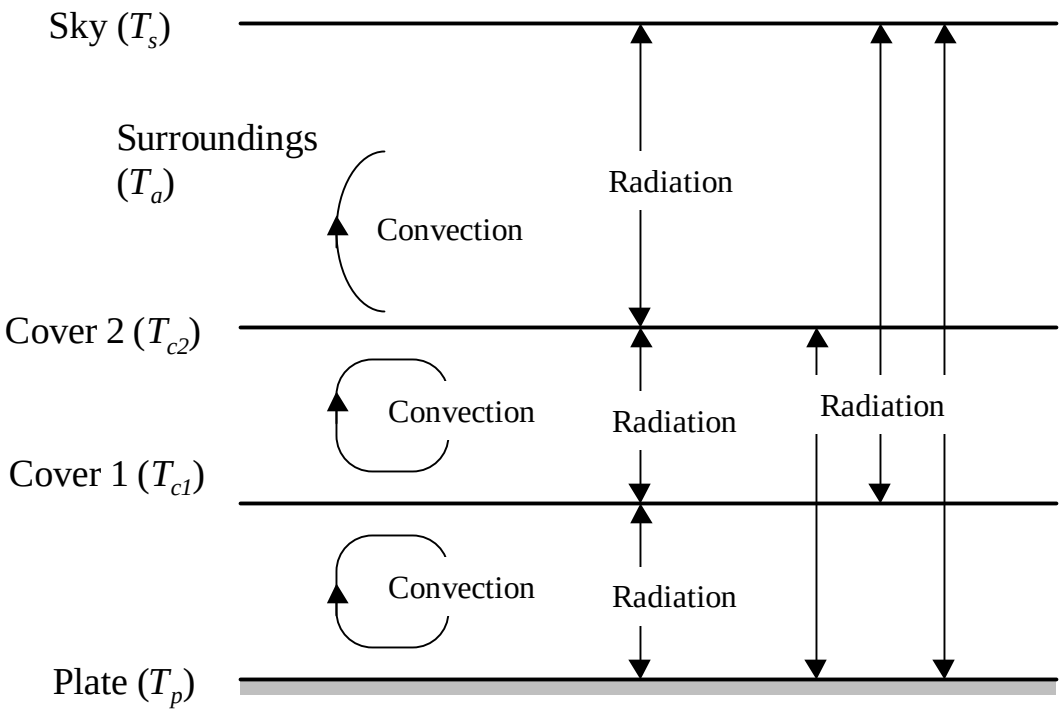

Figure 2.4.1 Heat transfer mechanisms through a cover system with two covers.

2.4.2.1 Cover-Plate System with No Covers

Figure 2.4.2 illustrates the top loss heat transfer mechanisms for the flat-plate collector with no covers. Heat is transferred by wind convection from the plate to ambient and by radiation to the sky

$$Q_t = Q_c + Q_r = h_w A_p \left(T_{pm} - T_a\right) + e_p s A_p \left(T_{pm}^4 - T_s^4\right) \qquad (2.4.3)$$

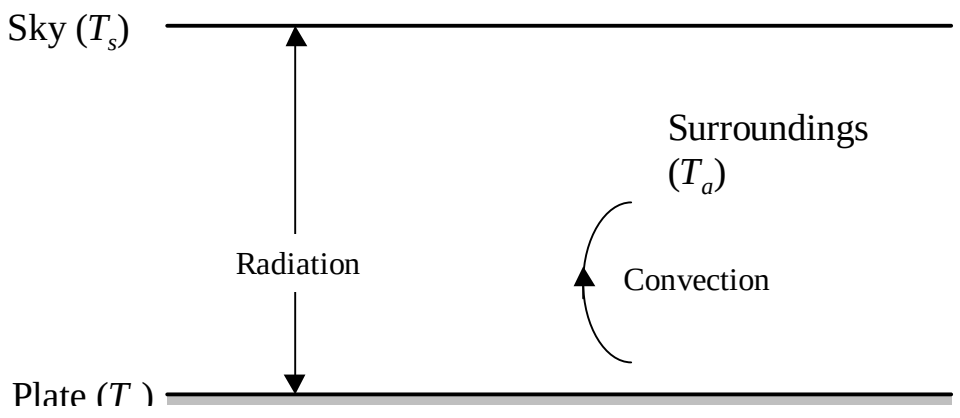

Figure 2.4.2 Top heat loss from the flat-plate solar collector with no covers

where subscripts *c* and *r* represent convection and radiation contribution, respectively. h_w is wind convection coefficient and T_s the sky temperature that will be discussed later. e_p is emittance of the absorber plate for infrared radiation and s is the Stefan-Boltzmann constant. Since the top heat loss occurs only at the absorber plate, the aperture area A_p is used with the assumption that the frontal transparent area is equal to the absorber area.

2.4.2.2 Cover-Plate System with One Cover

For a flat-plate solar collector with one cover, the top heat loss from the collector plate to the ambient can be obtained by applying the net-radiation method [12]. In Figure

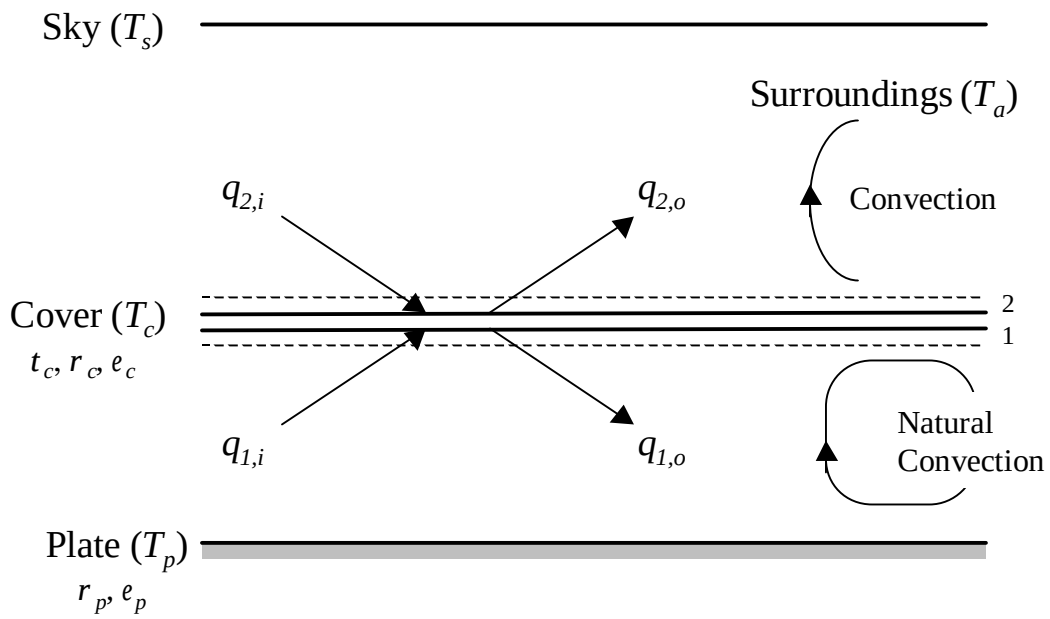

Figure 2.4.3 Net-radiation method applied to one cover-plate

Figure 2.4.3, the outgoing radiation flux from the cover can be written in terms of incoming fluxes as

$$q_{1,o} = t_c q_{2,i} + r_c q_{1,i} + e_c s T_c^4 \tag{2.4.4}$$

$$q_{2,o} = t_c q_{1,i} + r_c q_{2,i} + e_c s T_c^4 \tag{2.4.5}$$

where T_c is temperature of the cover. t_c, r_c, and e_c are transmittance, reflectance, and emittance of the cover for infrared radiation, respectively. The incoming fluxes are related to outgoing fluxes by

$$q_{1,i} = r_p q_{1,o} + e_p s T_{pm}^4 \tag{2.4.6}$$

$$q_{2,i} = s T_s^4 \tag{2.4.7}$$

where r_p and e_p are infrared reflectance and emittance of the plate, respectively. Applying energy conservation to the control volume around the cover and considering natural convection heat transfer between the cover and plate and wind convection heat transfer between the cover and surroundings yield

$$q_{1,i} - q_{1,o} + h_{c,pc}\left(T_{pm} - T_c\right) = q_{2,o} - q_{2,i} + h_w\left(T_c - T_a\right) \tag{2.4.8}$$

where $h_{c,pc}$ is natural convection heat transfer coefficient between the absorber plate and cover that will be discussed later. By solving Equations 2.4.4-2.4.8 simultaneously, heat fluxes and cover temperature can be obtained for the given temperatures of plate and sky and optical properties of cover-plate system. Top heat loss is the heat flux at the control surface times absorber area given by

$$Q_t = A_p \left[q_{1,i} - q_{1,o} + h_{c,pc} \left(T_{pm} - T_c \right) \right]. \tag{2.4.9}$$

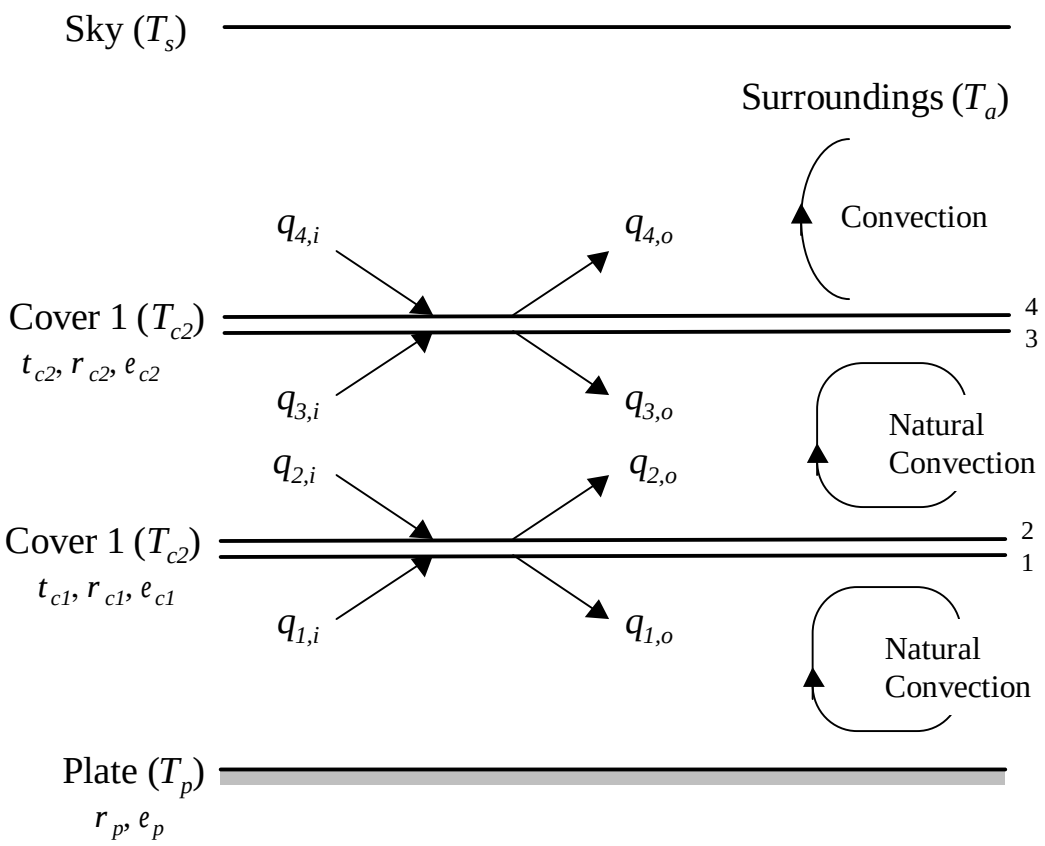

Figure 2.4.4 Net-radiation method for two cover-plate

2.4.2.3 Cover-Plate System with Two Covers

Figure 2.4.4 illustrates the net radiation method [12] for a flat-plate solar collector with two covers used to derive the expression for the top heat loss from the collector plate to ambient. The outgoing radiation flux from the covers can be written in terms of incoming fluxes as

$$q_{1,o} = t_{c1} q_{2,i} + r_{c1} q_{1,i} + e_{c1} s T_{c1}^4 \tag{2.4.10}$$

$$q_{2,o} = t_{c1} q_{1,i} + r_{c1} q_{2,i} + e_{c1} s T_{c1}^4 \tag{2.4.11}$$

$$q_{3,o} = t_{c2} q_{4,i} + r_{c2} q_{3,i} + e_{c2} s T_{c2}^4 \tag{2.4.12}$$

$$q_{4,o} = t_{c2} q_{3,i} + r_{c2} q_{4,i} + e_{c2} s T_{c2}^4 \tag{2.4.13}$$

where subscripts *c1* and *c2* represent cover 1 (inner cover) and cover 2 (outer cover). The incoming fluxes are related to outgoing fluxes by

$$q_{1,i} = r_p q_{1,o} + e_p s T_{pm}^4 \tag{2.4.14}$$

$$q_{2,i} = q_{3,o} \tag{2.4.15}$$

$$q_{3,i} = q_{2,o} \tag{2.4.16}$$

$$q_{4,i} = s T_s^4 \tag{2.4.17}$$

Applying the energy balance to two covers yields

$$q_{1,i} - q_{1,o} + h_{c,pc1}\left(T_{pm} - T_{c1}\right) = q_{2,o} - q_{2,i} + h_{c,c1c2}\left(T_{c1} - T_{c2}\right) \tag{2.4.18}$$

$$q_{3,i} - q_{3,o} + h_{c,c1c2}\left(T_{c1} - T_{c2}\right) = q_{4,o} - q_{4,i} + h_{w}\left(T_{c2} - T_{a}\right) \tag{2.4.19}$$

where $h_{c,pc1}$ and $h_{c,c1c2}$ are natural convection heat transfer coefficients between the plate and cover 1 and between cover 1 and cover 2, respectively. By solving Equations 2.4.10-2.4.19 simultaneously, all the radiation fluxes and cover temperatures can be obtained for the given values of plate and sky temperatures. The top loss from the plate to the ambient can be calculated from

$$Q_t = A_p\left[q_{c1,1,i} - q_{c1,1,o} + h_{c,pc1}\left(T_{pm} - T_{c1}\right)\right] \tag{2.4.20}$$

2.4.2.4 Sky Temperature

The radiation heat transfer from the plate to sky accounts for radiation exchange with the sky at sky temperature T_s rather than the ambient temperature T_a. The sky can be considered as a blackbody at some equivalent sky temperature T_s to account for the facts that the atmosphere is not a uniform temperature and that the atmosphere radiates only in certain wavelength band [3]. It can be calculated using the equation as follows [3]:

$$T_s = T_a\left[0.711 + 0.0056T_{dp} + 0.000073T_{dp}^2 + 0.013\cos(15t)\right]^{1/4}. \qquad (2.4.21)$$

where t is hour from midnight. T_s and T_a are in degrees Kelvin and T_{dp} is the dew point temperature in degrees Celsius.

2.4.2.5 Wind Convection Coefficient

Wind convection coefficient h_w represents the convection heat loss from a flat plate exposed to outside winds. It is related to three dimensionless parameters, the Nusselt number *Nu*, the Reynolds number *Re*, and the Prandtl number *Pr*, that are given

by [3]

$$Nu = \frac{h_w L_e}{k}, \qquad \mathrm{Re} = \frac{V L_e}{n}, \qquad \mathrm{Pr} = \frac{n}{a} \tag{2.4.22}$$

where the characteristic length L_e is four times the plate area divided by the plate perimeter, V wind speed. k, n, and a are the thermal conductivity, kinematic viscosity, thermal diffusivity of air.

For free standing collectors, Duffie and Beckman [3] suggests that the wind convection coefficient be calculated using the correlation of Sparrow over the Reynolds number range of 2×10^4 to 9×10^4:

$$Nu = 0.86\,\mathrm{Re}^{1/2}\,\mathrm{Pr}^{1/3} \qquad (2\times10^4<\mathrm{Re}<10^6). \tag{2.4.23}$$

For laminar flow, the correlation of Pohlhausen is used:

$$Nu = 0.86\,\mathrm{Re}^{1/2}\,\mathrm{Pr}^{1/3} \qquad (\mathrm{Re}<2\times10^4). \tag{2.4.24}$$

2.4.2.6 Natural Convection between Parallel Plates

For the prediction of the top loss coefficient, the evaluation of natural convection heat transfer between two parallel plates tilted at some angle to the horizon is of obvious importance. The natural convection heat transfer coefficient h_c is related to three dimensionless parameters, the Nusselt number *Nu*, the Rayleigh number *Ra*, and the Prandtl number *Pr*, that are given by

$$Nu = \frac{h_c L}{k}, \qquad Ra = \frac{g\beta_v \Delta T L^3}{\nu\alpha}, \qquad \Pr = \frac{\nu}{\alpha} \tag{2.4.25}$$

where L is the plate spacing, g the gravitational constant, ΔT the temperature difference between plates, and β_v is the volumetric coefficient of expansion of air.

Hollands et al. [4] suggested the relationship between the Nusselt number and Rayleigh number for tilt angle β from 0 to 75^o as

$$Nu = 1 + 1.44\left[1 - \frac{1708[\sin(1.8\beta)]^{1.6}}{Ra\cos\beta}\right]\left[1 - \frac{1708}{Ra\cos\beta}\right]^{+} + \left[\left(\frac{Ra\cos\beta}{5830}\right)^{1/3} - 1\right]^{+} \tag{2.4.26}$$

While Equation 2.4.26 is for the isothermal plates, plastic covers are thin and have low values of conductivity. Thus, the convection cells cause small temperature gradients along the covers. Yiqin et al. [21] suggested the following relationship for the natural convection for a two-cover system with the inner cover made from plastic:

$$Nu = 1 + 1.44\left[1 - \frac{1296[\sin(1.8b)]^{1.6}}{Ra\cos b}\right]\left[1 - \frac{1296}{Ra\cos b}\right]^{+} + \left[\left(\frac{Ra\cos b}{5830}\right)^{1/3} - 1\right]^{+}. \qquad (2.4.27)$$

2.4.3 Back and Edge Heat Loss

The energy loss through the back of the collector is the result of the conduction through the back insulation and the convection and radiation heat transfer from back of the collector to surroundings. Since the magnitudes of the thermal resistance of convection and radiation heat transfer are much smaller than that of conduction, it can be assumed that all the thermal resistance from the back is due to the insulation [3]. The back heat loss, Q_b, can be obtained from

$$Q_b = \frac{k_b}{L_b} A_c \left(T_{pm} - T_a \right) \tag{2.4.28}$$

where k_b and L_b are the back insulation thermal conductivity and thickness, respectively.

While the evaluation of edge losses is complicated for most collectors, the edge loss in a well-constructed system is intended to be so small that it is not necessary to predict it with great accuracy [3]. With the assumption of one-dimensional sideways heat flow around the perimeter of the collector, the edge losses can be estimated by

$$Q_e = \frac{k_e}{L_e} A_e \left(T_{pm} - T_a \right) \tag{2.4.29}$$

where k_e and L_e are the edge insulation thermal conductivity and thickness and A_e is edge area of the collector.

2.4.4 Overall Heat Loss Coefficient

The overall loss coefficient U_L based on the gross collector area can be calculated from Equation 2.4.1 with the known values of the overall heat loss Q_{loss} and the plate temperature T_{pm}. To derive an expression for the mean temperature of the absorber plate, it is necessary to know the overall heat loss coefficient based on the absorber area. Since of heat transfer coefficient-area product is constant, it can be calculated from

$$U_L' A_p = U_L A_c . \tag{2.4.30}$$

where $U¢_L$ is the modified overall heat loss coefficient whose base area is the aperture area of the collector.

2.5 The Mean Absorber Plate Temperature*

To calculate the collector useful gain using Equation 2.2.1, it is necessary to know the mean temperature of absorber plate that is a complicated function of the temperature distribution on the absorber plate, bond conductivity, heat transfer inside of

tubes and geometric configuration. To consider these factors along with the energy collected at the absorber plate and heat loss, the collector efficiency factor and the collector heat removal factor are introduced.

2.5.1 Collector Efficiency Factor

The collector efficiency factor, $F¢$ represents the temperature distribution along the absorber plate between tubes. Figure 2.5.1 illustrates the absorber plate-tube configuration of the present collector model. With the assumption of negligible temperature gradient in the fin in the flow direction, the collector efficiency factor can be obtained by solving the classical fin problem [3]. Figure 2.5.2(a) shows the fin with insulated tip that is to be analyzed. The plate just above the tube is assumed to be at some local base temperature T_b. The fin is (W-D)/2 long and has unit depth in the flow direction. By applying energy balance on the element shown in Figure 2.5.2(b), the

---

* The analysis follows the book, Solar Engineering of Thermal Processes, Duffie and Beckman, 1991 [3].

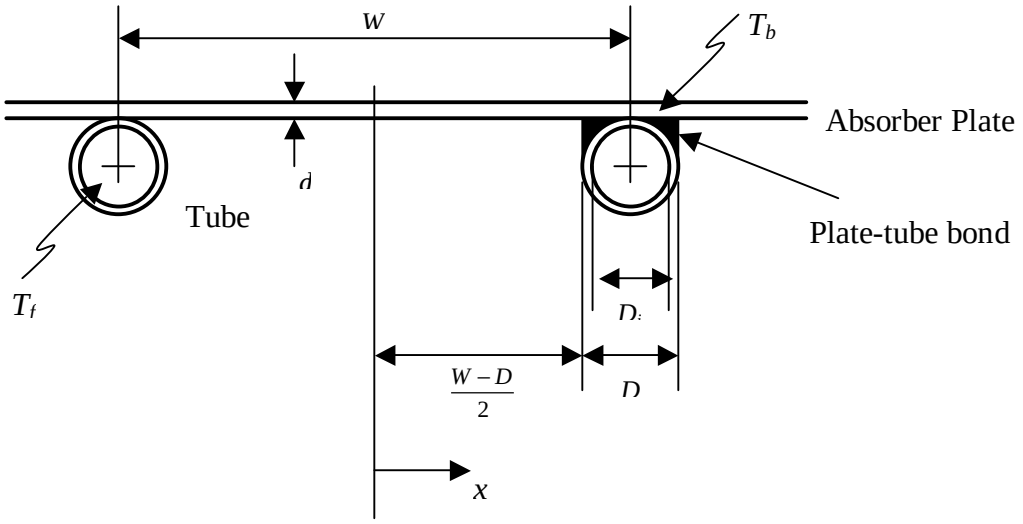

Figure 2.5.1 Geometric configuration of the absorber plate-tube

governing equation for the fin can be obtained as [3]:

$$\frac{d^2T}{dx^2} = \frac{U_L'}{kd}\left(T - T_a - \frac{S}{U_L'}\right). \tag{2.5.1}$$

where U_L is the overall loss coefficient based on the aperture area. The two boundary conditions are the insulated tip condition and the known base temperature T_b:

$$\left.\frac{dT}{dx}\right|_{x=0} = 0, \qquad T\big|_{x=\frac{W-D}{2}} = T_b. \tag{2.5.2}$$

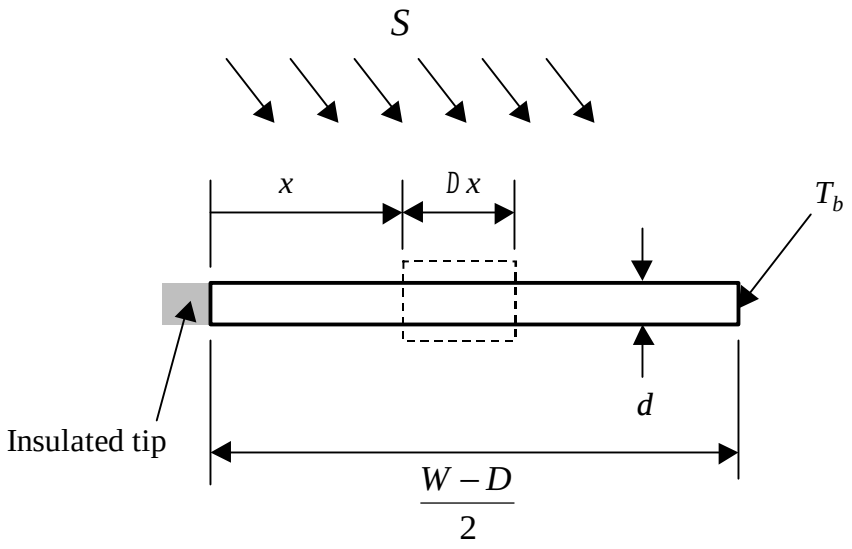

(a) fin with insulated tip

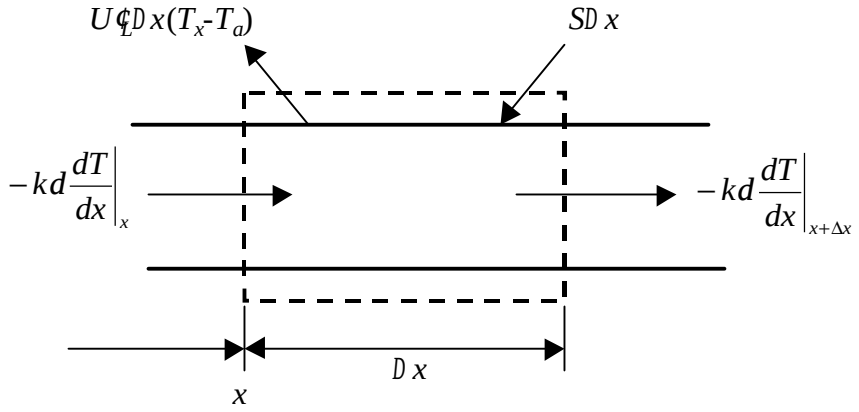

(b) energy balance on finite element

Figure 2.5.2 Fin configuration and energy balance

The energy transferred from the fin per unit of length in the flow direction can be found by applying Fourier's law to the fin base by considering the energy collected on the both sides of a tube:

$$q'_{fin} = (W - D)F\left[S - U'_L(T_b - T_a)\right] \tag{2.5.3}$$

where F is the fin efficiency for straight fins with rectangular cross section and defined

as

$$F = \frac{\tanh\left[m(W-D)/2\right]}{m(W-D)/2} \tag{2.5.4}$$

and m is a parameter of the fin-air arrangement defined as

$$m = \sqrt{\frac{U_L'}{kd}} \tag{2.5.5}$$

The solar energy absorbed just above the tube per unit of length in the flow direction can be calculated by

$$q'_{tube} = D\left[S - U_L'(T_b - T_a)\right]. \tag{2.5.6}$$

Then the useful gain q'_u per unit of depth in the flow direction is the sum of q'_{fin} and q'_{tube}:

$$q'_u = \left[(W-D)F + D\right]\left[S - U_L'(T_b - T_a)\right] \tag{2.5.7}$$

The thermal resistance to heat flow from the plate to the fluid results from the plate-tube bond conductance and the tube-to-fluid convection heat transfer inside of tubes. The useful gain per unit of length in the flow direction can be expressed as

$$q'_u = \frac{T_b - T_f}{\frac{1}{h_{fi} p D_i} + \frac{1}{C_b}} \tag{2.5.8}$$

where D_i is the inner diameter of a tube, h_{fi} the forced-convection heat transfer coefficient inside of tubes, T_f the local fluid temperature and C_b the bond conductance. By eliminating T_b from Equations 2.5.7 and 2.5.8 and by introducing the collector efficiency factor F' yields an expression for the useful gain as

$$q'_u = WF'\left[S - U'_L\left(T_f - T_a\right)\right] \tag{2.5.9}$$

where the collector efficiency factor F' is defined as

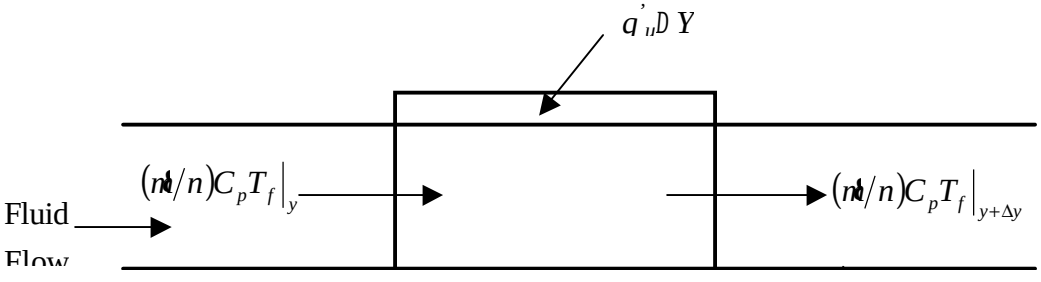

Figure 2.5.3 Energy balance of a control volume of the tube

$$F' = \frac{1/U_L'}{W\left[\frac{1}{U_L'[D+(W-D)]F} + \frac{1}{C_b} + \frac{1}{pD_i h_{fi}}\right]}. \qquad (2.5.10)$$

2.5.2 Temperature Distribution in Flow Direction

The fluid temperature of fluid varies along the tube with a certain temperature profile. Equation 2.5.9 expresses the useful gain per unit length in the flow direction as

a function of local fluid temperature that is a function of a position *y* along the flow direction. Applying the energy conservation to the control volume shown in Figure 2.5.3 and substituting Equation 2.5.9 for q'_u yield energy balance equation:

$$\frac{\dot{m}C_p}{nWF'}\frac{dT_f}{dy} - \left[S - U'_L\left(T_f - T_a\right)\right] = 0 \tag{2.5.11}$$

where $\dot{m}$ is the total collector flow rate, *n* the number of tubes, and T_f the temperature of fluid at any location *y*. With the assumption that F' and U_L are independent of position the fluid temperature at any position *y* can be calculated from

$$\frac{T_f - T_a - S/U'_L}{T_i - T_a - S/U'_L} = \exp\left(-\frac{U'_L nWF'y}{\dot{m}C_p}\right). \tag{2.5.12}$$

where T_i is fluid inlet temperature.

2.5.3 Collector Heat Removal Factor

The collector heat removal factor, F_R, is the ratio of the actual useful energy gain of a collector to the maximum possible useful gain if the whole collector surface were at the fluid inlet temperature. It is defined as

$$F_R = \frac{\dot{m} C_p (T_o - T_i)}{A_p [S - U_L' (T_i - T_a)]} \tag{2.5.13}$$

where the aperture area A_p is used as a reference area for the useful gain from the collector. The exit temperature T_o can be calculated using Equation 2.5.12 by substituting tube length L for y. Then Equation 2.5.13 can be expressed as [3]

$$F_R = \frac{\dot{m} C_p}{A_p U_L'} \left[1 - \exp\left(\frac{A_p U_L' F'}{\dot{m} C_p} \right) \right] \tag{2.5.14}$$

Physically the collector heat removal factor is equivalent to the effectiveness of a conventional heat exchanger. By introducing the collector heat removal factor and the

modified overall heat transfer coefficient into Equation 2.2.4, the actual useful energy gain Q_u can be represented as

$$Q_u = A_p F_R [S - U'_L (T_i - T_a)]^+ . \quad (2.5.15)$$

Introducing Equation 2.2.3 and 2.2.5 into Equation 2.5.15 yields

$$Q_u = A_c F_R [S_c - U_L (T_i - T_a)]^+ \quad (2.5.16)$$

Using Equations 2.5.15 and 2.5.16, the useful energy gain can be calculated as a function of the inlet fluid temperature not the mean plate temperature.

2.5.4 Mean Fluid and Plate Temperatures

For accurate the prediction of collector performance, it is necessary to evaluate properties of the working fluid to calculate the forced convection heat transfer coefficients inside of tubes and the overall loss coefficient. The mean fluid temperature T_{fm} at which the fluid properties are evaluated can be obtained by [3]:

$$T_{fm} = T_i + \frac{Q_u / A_p}{F_R U_L'}(1 - F'').$$ (2.5.17)

where the collector flow factor F'', defined as the ratio of F_R to F', are given by

$$F'' = \frac{F_R}{F'} = \frac{\dot{m} C_p}{A_p U_L' F'}\left[1 - \exp\left(\frac{A_p U_L' F'}{\dot{m} C_p}\right)\right]$$ (2.5.18)

The collector flow factor is a function of the dimensionless collector capacitance rate $\dot{m} C_p / A_p U_L F'$.

The mean plate temperature, T_{pm}, is always greater than the mean fluid temperature due to the heat transfer resistance between the absorbing surface and the fluid. Equating Equations 2.2.4 and 2.5.15 and solving for the mean plate temperature T_{pm} yields

$$T_{pm} = T_i + \frac{Q_u / A_p}{F_R U_L'}(1 - F_R)$$ (2.5.19)

2.5.5 Forced Convection inside of Tubes

For fully developed turbulent flow inside of tubes (Re>2300), the Nusselt number can be obtained from Gnielinsky correlation [5]:

$$Nu_{long} = \frac{(f/8)(Re_{tube} - 1000)Pr}{1 + 12.7\sqrt{f/8}\left(Pr^{2/3} - 1\right)} \tag{2.5.20}$$

where Darcy friction factor f for smooth surface is calculated from Petukhov relation [5] given by

$$f = \left(0.0790 \ln \mathrm{Re}_{tube} - 1.64\right)^{-2}. \tag{2.5.21}$$

For short tubes with a sharp-edged entry, the developing thermal and hydrodynamic boundary layers will result in a significant increase in the heat transfer coefficient near entrance. To consider this phenomena Duffie and Beckman [3] suggests that the

McAdams relation be used:

$$Nu = Nu_{long}\left[1+\left(\frac{D}{L}\right)^{0.7}\right] \tag{2.5.22}$$

where D and L is inner diameter and length of a tube.

For laminar flow inside of tubes the local Nusselt number for the case of short tubes and constant heat flux is given by [3]

$$Nu = Nu_{long} + \frac{a\left(RePrD/L\right)^{m}}{1+b\left(RePrD/L\right)^{n}}. \tag{2.5.23}$$

With the assumption that the flow inside of tubes is fully developed, the values of Nu_{long}, a, b, m, and n are 4.4, 0.00172, 0.00281, 1.66, and 1.29, respectively, for the constant heat flux boundary condition.

The friction factor f for fully developed laminar flow inside of a circular tube can be calculated from

$$f = \frac{64}{\mathrm{Re}_D}. \tag{2.5.24}$$

Generally the straight tubes are connected headers on both ends that provide pipe entrance and exit with sharp edges. The friction coefficients for those minor losses are approximated by

$$f_{\min or} L_{eq} = KD \tag{2.5.25}$$

where L_{eq} is equivalent length and K loss coefficient. The value of loss coefficient is 0.5 for entrance with sharp edge and 1.0 for pipe exit [20]. Then the pressure drop through a pipe and header can be calculated by

$$\Delta P = f_{pipe}\left(\frac{r_f U^2}{2D}\right)L + \sum K\left(\frac{r_f U^2}{2}\right) \tag{2.5.26}$$

where U represents the mean fluid velocity inside of the tube and r_f is fluid density.

2.6 Thermal Performance Of The Collectors

Based on the analysis in the previous sections, the thermal performance of the flat-plate collector can be calculated. The thermal performance of the collector can be represented by the instantaneous efficiency and the incidence angle modifier. The stagnation temperature is also needed to ensure that the collector materials do not exceed their thermal limit.

2.6.1 Instantaneous Efficiency

The instantaneous collector efficiency, h_i, is a measure of collector performance that is defined as the ratio of the useful gain over some specified time period to the incident solar energy over the same time period:

$$h_i = \frac{\int Q_u dt}{A_c \int G_T dt}. \qquad (2.6.1)$$

where G_T is the intensity of incident solar radiation. According to ASHRAE Standard 93-86 [1], the gross area A_c is used as a reference collector area in the definition of instantaneous efficiency. By introducing the Equation 2.5.16, the instantaneous efficiency becomes

$$h_i = \frac{Q_u}{A_c G_T} = \left[F_R(ta) - F_R U_L \frac{(T_i - T_a)}{G_T} \right]^+ . \tag{2.6.2}$$

where the absorbed energy S_c based on the gross collector area has been replaced by

$$S_c = G_T(ta). \tag{2.6.3}$$

(ta) is the effective transmittance-absorptance product based on the collector gross area defined as

$$(ta) = \frac{SA_p}{G_T A_c} = (ta)_{avg} \frac{A_p}{A_c} \tag{2.6.4}$$

where $(\tau\alpha)_{avg}$ is the transmittance-absorptance product averaged for beam, diffuse, and ground-reflected irradiation. SA_p is the solar energy absorbed at absorber surface and $G_T A_c$ is the total solar energy incident on the gross area of the collector. In Equation 2.6.2, two important parameters, $F_R(\tau\alpha)$ and $F_R U_L$, describe how the collector works. $F_R(\tau\alpha)$ indicates how energy is absorbed by the collector while $F_R U_L$ is an indication of how energy is lost from the collector.

2.6.2 Incidence Angle Modifier

To express the effects of the angle of incidence of the radiation on thermal performance of the flat-plate solar collector, an incidence angle modifier $K_{\tau\alpha}$ is employed [1]. It describes the dependence of $(\tau\alpha)$ on the angle of incidence of radiation on the collector and is a function of the optical characteristics of covers and the absorber plate. It is defined as

$$K_{ta} = \frac{(ta)}{(ta)_n} \tag{2.6.5}$$

where subscript *n* indicates that the transmittance-absorptance product is for the normal incidence of solar radiation.

2.6.3 Stagnation Temperatures

A plastic cover will melt when the temperature of the cover exceeds its melting point. To ensure the thermal tolerance of the collector, the highest temperature in the collector should be less than the melting point of the plastic covers. Stagnation temperatures are the highest temperatures of the covers and absorber plate that can be obtained from the collector. They occur when the collector is not working, that is, when the working fluid does not circulate. In this case, the useful gain from the collector is zero in Equation 2.2.1 and then the energy balance equation becomes

$$A_p S = A_c U_L (T_{pm} - T_a) \tag{2.6.6}$$

By solving this equation with the constitutive equations provided in this chapter, the stagnation temperatures can be obtained.

2.7 Collector Test And Thermal Performance Models

In this study the thermal performance test of flat-plate collector consists of three parts. The first is to determine instantaneous efficiency with beam radiation nearly normal to the absorber surface. The second is determination of incident angle modifier. The last is determination of the stagnation temperature. This section briefly reviews the standard test procedure and introduces the thermal performance models for the instantaneous efficiency and incidence angle modifier.

2.7.1 Instantaneous Efficiency

The ASHRAE Standard 93-86 [1] and SRCC document RM-1 [17] provide the standard test methods for flat-plate solar collectors. The general test procedure is to operate the collector in a test facility under nearly steady conditions and measure the data that are needed for analysis. Although details differ, the essential features of all of the procedures can be summarized as below [3]:

1. Solar radiation is measured by a pyranometer in the plane of the collector.
2. Flow rate of working fluid, inlet and outlet fluid temperatures, ambient temperature, and wind speed) are measured.
3. Tests are made over a range of inlet temperatures.
4. The inlet pressure and pressure drop in the collector are measured.

Information available from the test is data on the thermal input, data on the thermal output, and data on the ambient conditions. These data characterize a collector by parameters, $F_R(\tau\alpha)$, and $F_R U_L$, that indicate absorption of solar energy and energy loss

from the collector.

Instantaneous efficiencies can be determined from

$$h_i = \frac{Q_u}{A_c G_T} = \frac{\dot{m} C_p (T_o - T_i)}{A_c G_T} \tag{2.7.1}$$

where T_o is the exit temperature of the working fluid. The instantaneous efficiency can be presented in three ways; one linear model and two second-order models:

$$h_i = a_1 - a_2 \frac{(T_i - T_a)}{G_T} \tag{2.7.2}$$

$$h_i = a_3 + a_4 \frac{(T_i - T_a)}{G_T} + a_5 \left[\frac{(T_i - T_a)}{G_T} \right]^2 \tag{2.7.3}$$

$$h_i = a_6 + a_7 \frac{(T_i - T_a)}{G_T} + a_8 \frac{(T_i - T_a)^2}{G_T} \tag{2.7.4}$$

With the test data over a range of inlet temperatures, the instantaneous efficiency can be plotted as a function of $(T_i\text{-}T_a)/G_T$. The coefficients of Equations 2.7.2 – 2.7.4 can be found by linear regression.

European practice employs $(T_{f,av}\text{-}T_i)/G_T$ as a base of collector test results where

$T_{f,av}$ is the arithmetic average of the fluid inlet and outlet temperature

2.7.2 Incidence Angle Modifier

The second important aspect of collector testing is the determination of effects of incident angle of the solar radiation. The standard test methods [1,17] include experimental estimation of this effect and require a clear test day so that the experimental value of $(\tau\alpha)$ is essentially the same as $(\tau\alpha)_b$. ASHRAE Standard 93-86 [1] recommends that experimental determination of $K_{\tau\alpha}$ be done with the incidence angles of beam radiation of 0, 30, 45, 60°.

For flat-plate solar collector Souka and Safwat [16] have suggested an expression for angular dependence of $K_{\tau\alpha}$ as

$$K_{\tau\alpha} = 1 + b_0\left(\frac{1}{\cos\theta} - 1\right) \qquad (2.7.5)$$

where θ is angle of incidence of beam radiation and b_0 is the incidence angle modifier

coefficient. The incidence angle modifier coefficient can be determined using linear regression with the test data of K_{ta} over several values of incident angles.

CHAPTER THREE

RESULTS AND DISCUSSION

Provided that the calculation predicts the experimental results accurately, the design program for flat-plate solar collectors might substitute for the experimental test at the development level and enable the solar industries to make well-designed economical solar collectors. In this chapter the comparisons with the experimental test are performed and the effects of parameters are investigated.

3.1 Natural Convection Between Parallel Plates

The natural convection between the cover and plate and between covers plays an important role in top heat loss through a cover system. As explained in Section 2.4.2.6, the natural convection coefficients between two parallel plates can be calculated using two equations: Equation 2.4.26 for glass cover system and Equation 2.4.27 for the cover system with plastic as the inner cover.

Figure 3.1.1 shows Nusselt numbers as a function of Rayleigh number for natural convection heat transfer between parallel plates at various slopes. Solid curves are the calculation result from the equation of Hollands et al. [4] (Equation 2.4.26) and dotted curves are from Yiqin et al. [21] (Equation 2.4.27). Curves without symbols are for horizontal plates, Curves with hollow circles, hollow squares, solid circles are for the parallel plates tilted at 45^{o}, 60^{o}, and 75^{o} with respect to horizon, respectively. As shown in this figure the Nusselt number from Equation 2.4.13 is always larger than that from Equation 2.4.12. These results show that the small temperature gradient along the plastic cover caused by the convection cells enhances the natural convection heat transfer.

Figure 3.1.2 shows a comparison of collector efficiencies calculated with the two relations for natural convection heat transfer between the cover and plate and between covers. The collector configuration and test conditions are based on the FSEC solar collector test report for MSC-32 flat plate solar collector [13]. To investigate the effect of natural convection correlation, a polyvinylfluoride (tedlar) cover is used for the inner cover of the collector and the cover-to-cover air spacing is set to 0.5 cm. The optical properties of the plastic covers are given by

Solar Spectrum : Refractive Index =1.45

Transmittance = 0.9

Infrared Spectrum : transmittance = 0.3

Absorptance = 0.63

The equation of Yiqin et al. always yields a higher Nusselt number and thus its heat transfer coefficient exceeds that from Hollands et al. It causes the higher top loss coefficient and lower collector efficiency. Even though the difference in the two Nusselt

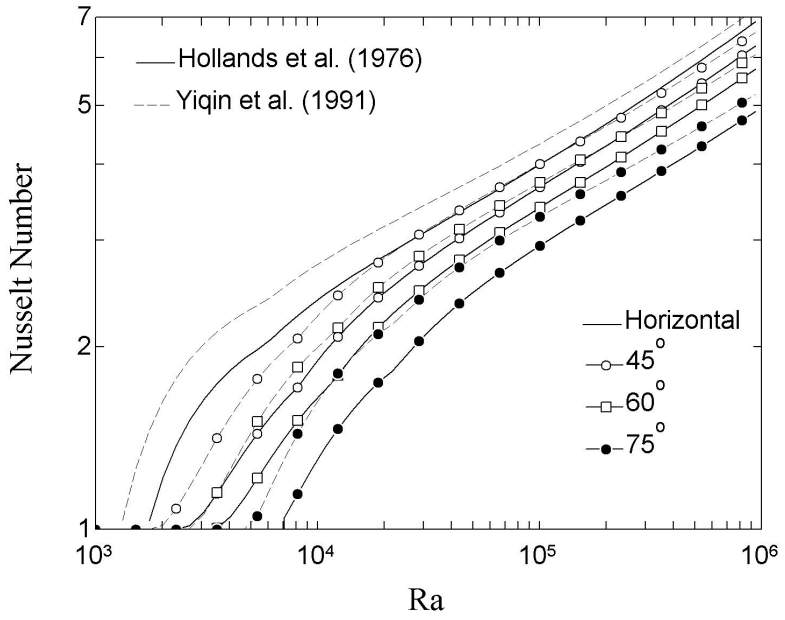

Figure 3.1.1 Nusselt numbers for natural convection heat transfer between parallel plates at various angles

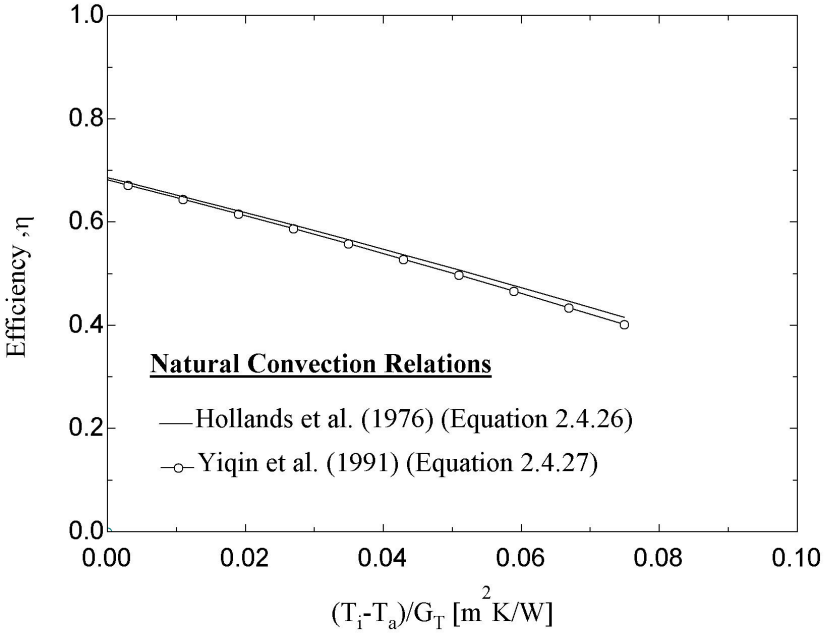

Figure 3.1.2 Comparison of Instantaneous efficiencies of the collector with different natural convection relations

numbers decreases with an increase of Rayleigh number (Figure 3.1.1), the difference in instantaneous efficiencies increases as the temperature difference increases (Figure 3.1.2). This indicates that the proportion of the total heat loss that is natural convection becomes larger as the absorber plate temperature increases. The Hollands et al. equation overpredicts the instantaneous efficiency of the collector.

3.2 Comparison With Experiments

The calculation results were compared with the experimental results from three flat-plate solar collectors. The experimental tests were performed by the Testing and Laboratories Division, Florida Solar Energy Center (FSEC) according to the SRCC testing method [17]. The calculations were performed with the test conditions and collector configuration provided by the test reports [13-15].

3.2.1 MSC-32 (American Energy Technologies, Inc.)

Figure 2.1.1 shows the detailed geometric configuration of the MSC-32 flat-plate solar collector [13]. Even though the detailed plate-tube configuration is different from that of Figure 2.2.2, the overall geometric configuration is similar to the general model. Test conditions and collector configurations provided by the FSEC test report are summarized at Table 3.2.1 [13]. The test conditions are averaged values of the experimental measurement.

A plot of the instantaneous efficiency of the MSC-32 collector as a function of $(T_i\text{-}T_a)/G_T$ is shown in Figure 3.2.1. The predicted instantaneous efficiency is compared to the experimental results from the test report. As shown in this figure, the calculation can predict the experimental results very well. The linear and 2nd-order polynomial efficiency equations with the calculated coefficients are

$$h_i = 0.746 - 4.33\frac{(T_i - T_a)}{G_T}, \qquad h_i = 0.743 - 3.98\frac{(T_i - T_a)}{G_T} - 4.99\left[\frac{(T_i - T_a)}{G_T}\right]^2$$

while those from experimental test [13] are given by

$$h_i = 0.751 - 4.45\frac{(T_i - T_a)}{G_T}, \qquad h_i = 0.736 - 2.96\frac{(T_i - T_a)}{G_T} - 20.65\left[\frac{(T_i - T_a)}{G_T}\right]^2.$$

Figure 3.2.2 compares the predicted incident angle modifier with the experiments. The calculated value of incidence angle modifier is -0.13 while the experiment yields -0.15. The calculated value of the incidence angle modifier coefficient has about a 13% error compared to the experimental result. For the calculation of angular dependence of the transmittance-absorptance product on incident

Table 3.2.1 Test conditions and specification of MSC-32 Flat plate solar collector

Test Conditions	Incident solar radiation		1000 [W/m^2]
	Diffuse radiation proportion		0 [%]
	Incident angle		0 [deg]
	Collector slope		45 [deg]
	Ambient temperature		20 [C]
	Wind speed		2 [m/s]
Collector Dimension	Overall dimension	Length	2.491 [m]
		Width	1.221 [m]

		Thickness	0.079 [m]
	Absorber dimension	Length	2.4 [m]
		Width	1.137 [m]
Cover	Number of Covers		1
	Material		Glass
	Solar Spectrum	Refractive Index	1.526
		Transmittance	0.891
	Infrared Spectrum	Absorptance	0.88
		Transmittance	0
Cover-Plate air spacing			1.8 [cm]
Plate	Material		Copper
	Conductivity		380 [W/mK]
	Thickness		0.02 [cm]
	Absorptance		0.95
	Emittance		0.1
Back & Edge Insulation	Back Insulation	Thickness	3.17 [cm]
		Conductivity	0.03 [W/mK]
	Edge Insulation	Thickness	3.17 [cm]
		Conductivity	0.03 [W/mK]
Tubes & Fluid	Number of tubes		10
	Inner diameter		1.6 [cm]
	Plate-tube bond conductivity		400 [W/mK]
	Working fluid		Water
	Volumetric flow rate		4.75 [L/min]
	Inlet pressure		200 [kPa]

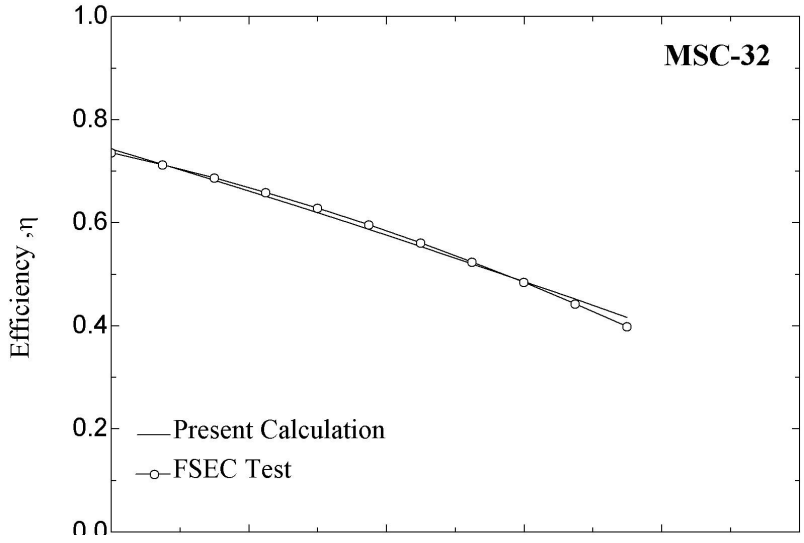

Figure 3.2.1 Comparison of calculated efficiency with experiment for MSC-32 flat-

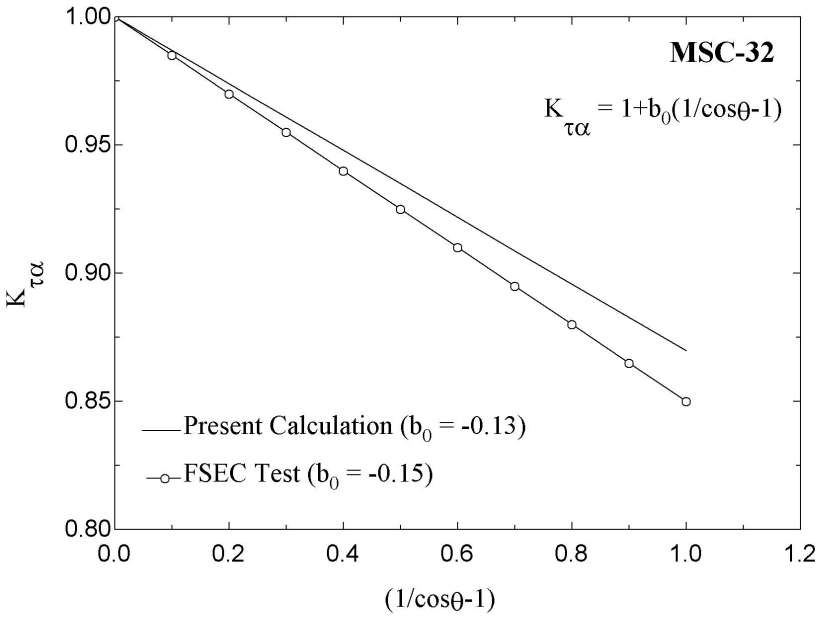

plate solar collector

Figure 3.2.2 Comparison of calculated incidence angle modifier with experiment for

MSC-32 flat-plate solar collector

angle, Equation 2.3.15 is employed as a model for the angular dependence of the absorptance of the absorber plate. Even though almost all selective surfaces may exhibit similar behavior, there might be difference between this generalized equation and the actual plates. This difference may cause the error in the predicted value of incidence angle modifier coefficient.

3.2.2 SX-600 (Solmax Inc.)

Table 3.2.2 shows test conditions and collector configurations for the Solmax SX-600 flat-plate solar collector based on the FSEC solar collector test report [15]. Figure 3.2.3 illustrates comparison of the predicted and experimental instantaneous efficiencies. As shown in the figure, the calculation can predict the experimental results very accurately. The calculated efficiency equations are

$$h_i = 0.741 - 6.87\frac{(T_i - T_a)}{G_T}, \qquad h_i = 0.733 - 5.95\frac{(T_i - T_a)}{G_T} - 12.83\left[\frac{(T_i - T_a)}{G_T}\right]^2.$$

Experimental efficiency equations [15] are given by

Table 3.2.2 Test conditions and specification of SX-600 Flat plate solar collector

Test Conditions	Incident solar radiation		1000 [W/m^2]
	Diffuse radiation proportion		0 [%]
	Incident angle		0 [deg]
	Collector slope		45 [deg]
	Ambient temperature		18 [C]
	Wind speed		2.5 [m/s]
Collector Dimension	Overall dimension	Length	2.494 [m]
		Width	1.232 [m]
		Thickness	0.095 [m]
	Absorber dimension	Length	2.432 [m]
		Width	1.170 [m]
Cover	Number of Covers		1
	Material		Glass
	Solar Spectrum	Refractive Index	1.526
		Transmittance	0.891
	Infrared Spectrum	Absorptance	0.88
		Transmittance	0
Cover-Plate air spacing			2.8 [cm]
Plate	Material		Copper
	Conductivity		380 [W/mK]
	Thickness		0.051 [cm]
	Absorptance		0.95

	Emittance		0.95
Back & Edge Insulation	Back Insulation	Thickness	3.8 [cm]
		Conductivity	0.03 [W/mK]
	Edge Insulation	Thickness	2.0 [cm]
		Conductivity	0.03 [W/mK]
Tubes & Fluid	Number of tubes		11
	Outer diameter		1.3 [cm]
	Plate-tube bond conductivity		100 [W/mK]
	Working fluid		Water
	Volumetric flow rate		3.4 [L/min]
	Inlet pressure		200 [kPa]

Figure 3

0 flat-plate solar coll

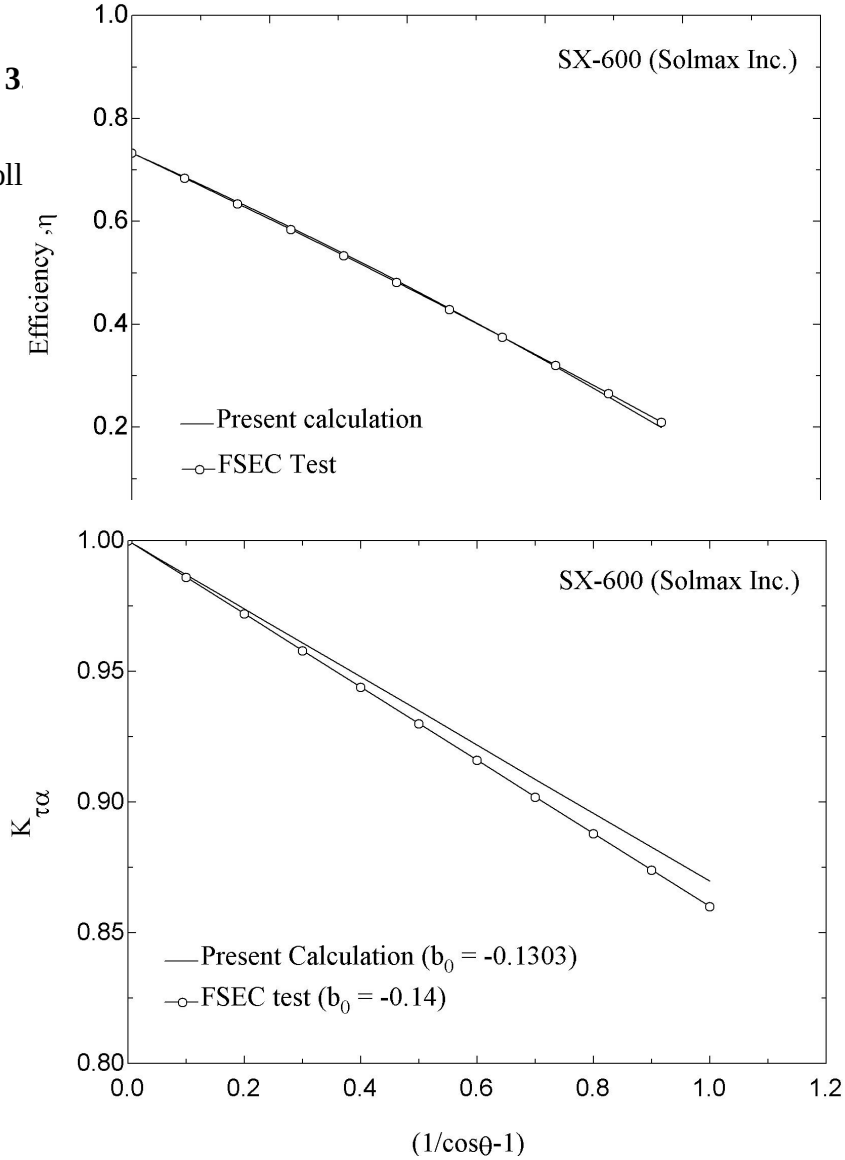

Figure 3.2.4 Comparison of calculated incidence angle modifier with experiment for SX-600 flat-plate solar collector

$$h_i = 0.737 - 6.77\frac{(T_i - T_a)}{G_T}, \qquad h_i = 0.733 - 6.28\frac{(T_i - T_a)}{G_T} - 6.82\left[\frac{(T_i - T_a)}{G_T}\right]^2.$$

Figure 3.2.4 shows the comparison of incidence angle modifier. The calculated value of incidence angle modifier is -0.13 while the experimental test yields -0.14, in good agreement with the experiment. However, the calculated value of incidence angle modifier is almost the same as the value of MSC-32. This similar values result from the fact that the fact that the calculations for both collectors employ the same model for the angular dependence of the optical property of the plate.

3.2.3 STG-24 (Sun Trapper Solar Systems, Inc.)

Table 3.2.3 summarizes test conditions and collector configurations of STG-24

flat-plate solar collector that is produced by Sun Trapper Solar Systems, Inc [14]. Figure 3.2.5 shows the calculated and experimental instantaneous efficiencies of the collector as a function of $(T_i\text{-}T_a)/G_T$. The curve with the conductivity of the back and edge insulation labeled k = 0.02 W/mK is the result of calculation with the values of Table 3.2.3. In this case, the instantaneous efficiency is overpredicted compared to the experimental results. However, as the value of the insulation conductivity increases, the predicted curve approaches the experimental result. The calculation yields the accurate experimental collector performance when k = 0.055 W/mK. There are two possibilities that cause this result. The first is that the value of back and edge insulation conductivity provided by manufacturer may be different from the actual value. The other possibility is that there might be a thermal leakage in this collector. The increase in back and edge thermal conductivity causes an increase in the heat loss from the collector and is equivalent to the increase of thermal leakage from the collector. This indicates that this flat-plate collector may not be a well-constructed collector. Figure 3.2.6 shows the incidence angle modifier as a function of $(1/\cos q\text{-}1)$. It also shows a good agreement of the calculation with the experiment.

From the comparison of the calculation results with the experimental results, it can be concluded that the flat-plate solar collector design program can accurately predict the thermal performance of flat-plate collectors with one glass cover. Since the test reports of the collector with two covers or plastic covers are not available, a direct comparison was not made. Since the analytical base of the solar collector design program developed in Chapter 2 has been verified by substantial experimental evidence [3], it can be concluded that the flat-plate solar collector design program developed in this study has an ability to predict the accurate performance of the collector.

Table 3.2.3 Test conditions and specification of STG-24 Flat plate solar collector

Test Conditions	Incident solar radiation		1000 [W/m^2]
	Diffuse radiation proportion		0 [%]
	Incident angle		0 [deg]
	Collector slope		45 [deg]
	Ambient temperature		30 [C]
	Wind speed		2 [m/s]
Collector Dimension	Overall dimension	Length	1.841 [m]
		Width	1.257 [m]
		Thickness	0.078 [m]
	Absorber dimension	Length	1.1789 [m]
		Width	1.201 [m]
Cover	Number of Covers		1
	Material		Glass
	Solar Spectrum	Refractive Index	1.526
		Transmittance	0.891
	Infrared Spectrum	Absorptance	0.88
		Transmittance	0
Cover-Plate air spacing			2.8 [cm]
Plate	Material		Aluminum
	Conductivity		177 [W/mK]
	Thickness		0.193 [cm]
	Absorptance		0.96
	Emittance		0.4
Back & Edge Insulation	Back Insulation	Thickness	2.5 [cm]
		Conductivity	0.02 [W/mK]
	Edge Insulation	Thickness	2.5 [cm]
		Conductivity	0.02 [W/mK]
Tubes & Fluid	Number of tubes		8
	Outer diameter		1.3 [cm]
	Plate-tube bond conductivity		400 [W/mK]
	Working fluid		Water
	Volumetric flow rate		2.6 [L/min]
	Inlet pressure		200 [kPa]

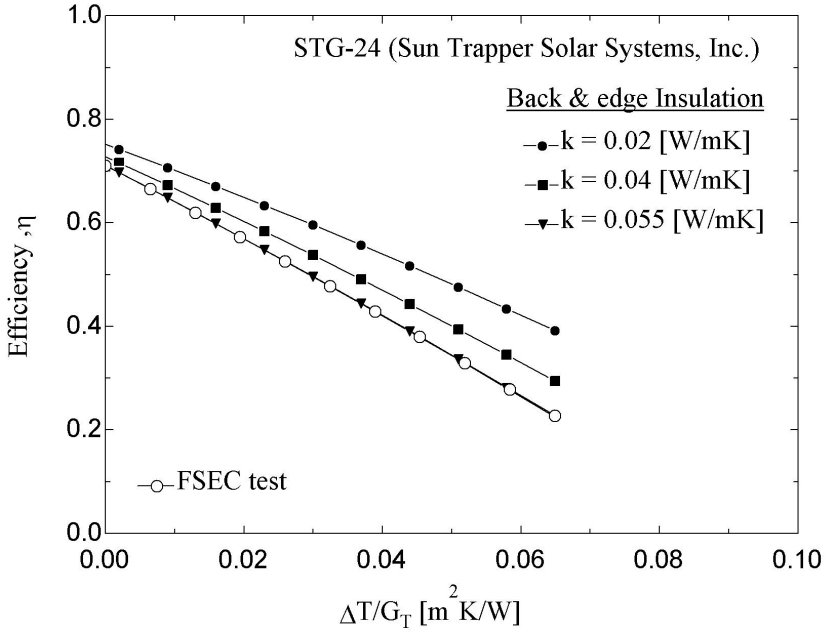

Figure 3.2.5 Comparison of calculated efficiency with experiment for STG-24 flat-plate solar c

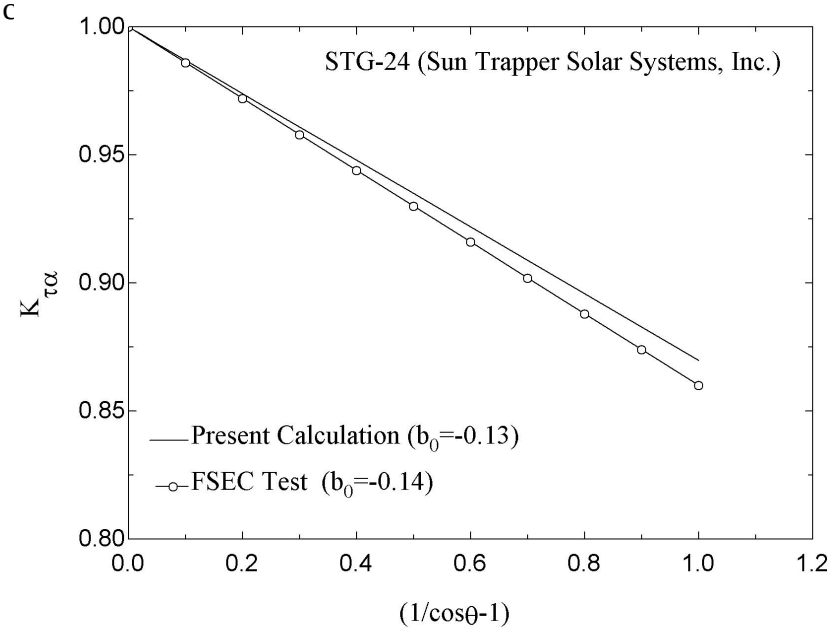

Figure 3.2.6 Comparison of calculated incidence angle modifier with experiment for STG-24 flat-plate solar collector

3.3 Effects Of Design Parameters

The design program was successfully verified in the last section. As a result it is possible to investigate the effect of design parameters by numerical simulation. In this section the effects of three design parameters on the collector efficiency are investigated. The test conditions and the collector configuration are based on those of MSC-32 test report (Table 3.2.1) [13].

3.3.1 Number of Covers

Figure 3.3.1 shows the effect of the number of covers on the collector instantaneous efficiency. In the case of two covers, they are assumed to be optically identical and the cover-to-cover air spacing is set to be 0.5 cm. In this figure, the value of intercept $F_R(\tau\alpha)$ decreases with the increase of the number of covers since the value of transmittance of the cover system decreases. The slope of curves, $F_R U_L$, decreases as the number of covers increases since the overall heat loss coefficient is a function of the mean plate temperature and ambient conditions and its dependence on the plate temperature decreases with the increasing number of covers.

3.3.2 Number of Tubes

The effect of the number of tubes on the instantaneous efficiency of the collector is illustrated in Figure 3.3.2. As the number of tubes increases, the tube-to-tube spacing W decreases and the collector heat removal factor F_R increases according to Equations 2.5.10 and 2.5.14 while the value of $(\tau\alpha)$ remains constant. Thus, the instantaneous efficiency improves with the increase of the number of tubes. The degree of improvement decreases and there exists the optimum number of tubes for the collector

considering the manufacturing cost. As shown in this figure the instantaneous efficiency for 11 tubes is almost identical to that for 10 tubes. Thus the optimum number of tubes is less than10 for MSC-32 collector.

3.3.3 Infrared Properties of the Cover

While the glass cover is opaque to infrared radiation the plastic cover is partially transparent. Figure 3.3.3 indicates the effect of infrared properties of the cover materials on the instantaneous efficiency of the collector. To investigate the effect of infrared properties of the cover, the optical properties in solar spectrum is assumed to be the same as those of glasses. The reflectance of the cover is set to 0.05. With the various values of transmittance and fixed value of reflectance, the absorptance of the cover is determined by Kirchhoff's law. With black paint absorber surface the efficiency decreases as the transmittance of the cover increases (Figure 3.3.3(a)) since top loss due to the direct radiation exchange between the plate and the sky increases. In the case of selective absorber plate, however, efficiency improves with the increase of transmittance of the cover as shown in Figure 3.3.3(b). In this case the natural

convection between the cover and the plate plays a more important role in top heat loss than radiation exchanger between them. As the infrared transmittance of the cover increases, the radiation heat transfer increases and the natural convection decreases. Since the degree of increase in radiation heat transfer between the cover and the plate is small compared to that of the natural convection heat transfer, the top loss from the plate decreases and the instantaneous efficiency improves. The infrared properties has an impact on the values of intercept, $F_R(ta)$, since F_R is a function of loss coefficient by Equation 2.5.14. The infrared radiation properties of the cover do not have much effect on efficiency when the infrared transmittance of the cover is less than 0.7 with selective absorber plate. More study is required to understand the exact physical mechanism related to the effect of infrared properties of the cover on the collector performance.

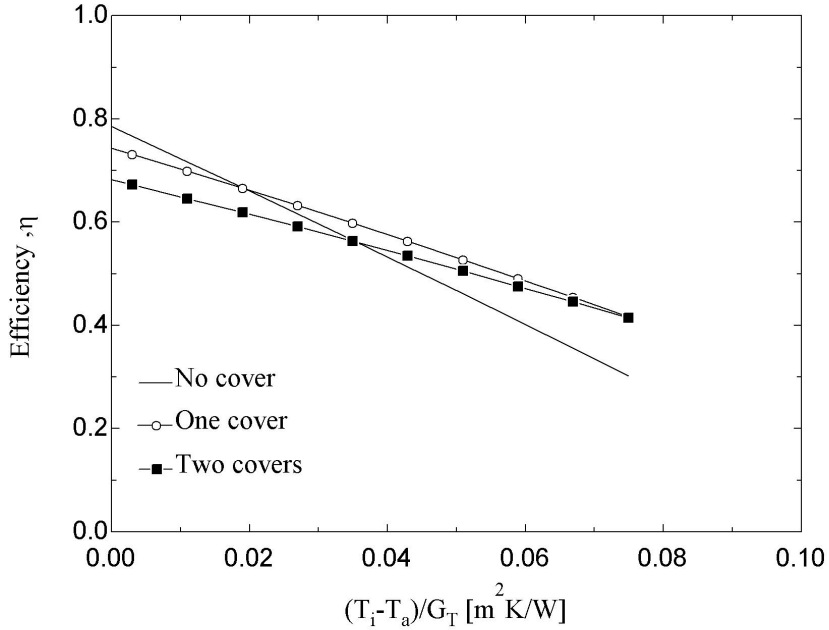

Figure 3.3.1 Effect of the number of covers on the collector efficiency

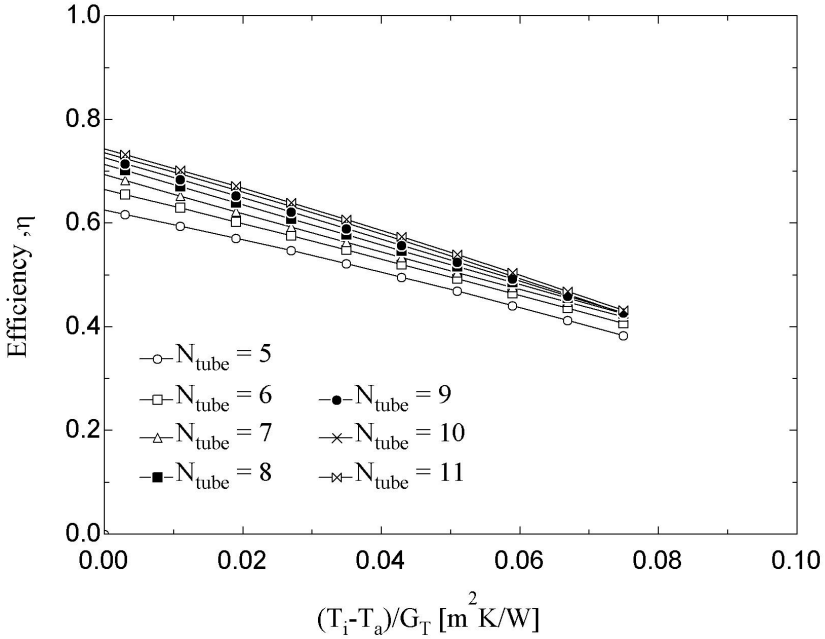

Figure 3.3.2 Effect of the number of tubes on the collector efficiency

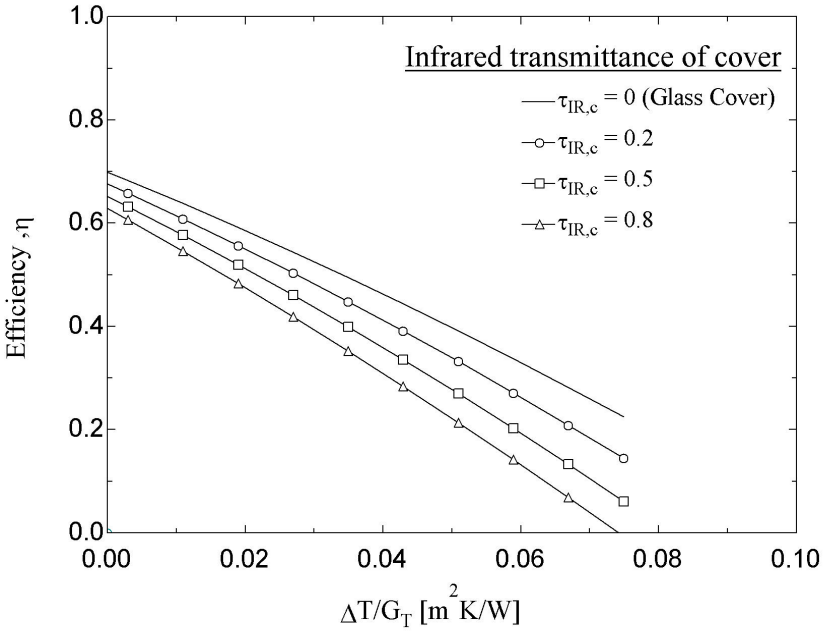

(a) Black absorber plate (e_p = 0.95)

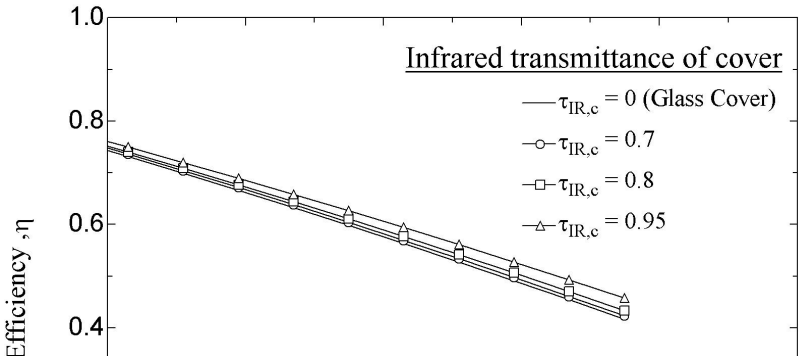

(b) Selective absorber plate (e_p = 0.1)

Figure 3.3.3 Effect of the infrared properties of cover on the collector efficiency

CHAPTER FOUR

CONCLUSIONS

An analytical and numerical study has been conducted to develop a design program for flat-plate solar collectors (CoDePro). The program is based on established theory about the radiation absorption, heat loss, and temperature distribution along the plate. Radiation absorption is calculated by using the transmittance-absorptance product

of the cover and plate system. In the evaluation of heat loss from the collector, the net radiation method was employed to calculate top loss for a general cover system. The correlation of Yiqin et al. [21] was employed for natural convection heat transfer for the cover system with plastic as the inner cover. For other cover configurations the correlation of Hollands et al. [4] was used. The temperature distribution along the plate was represented by the collector heat removal factor. In the analysis the aperture area of the collector is used to consider the effect of the edge of collector frontal surface.

In this study, the semi-gray radiation model was employed for the optical properties of the collector covers. The optical properties of the cover system for infrared radiation were assumed to be diffuse radiation properties that can be obtained by using ray-tracing techniques.

Comparisons of the calculated results with the experiments indicate that the design program developed in this study has an ability to predict the thermal performance of the collector. The predicted instantaneous efficiency of the collector is almost the same as the experimental results while there is a little discrepancy between the calculated and experimental values of incidence angle modifier coefficient. The error in incidence angle modifier may come from the lack of information about the

optical properties of the absorber plate.

Through this study a design program for flat-plate solar collector has been developed so that very detailed information can be specified to allow solar engineers to investigate the impact of various design changes on collector performance. The program has been distributed to solar engineers and modified according to their suggestions. It has an easy-to-use graphical interface and provides an accurate prediction of the thermal performance of the collector. Thus, it can be concluded that the program can be used as a design tool for a company specializing in solar systems to investigate the impact of design parameters. It can also be used as a tool for identifying design problems.